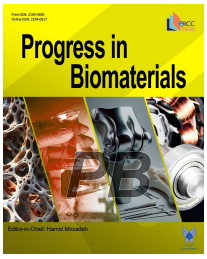

Progress. in Biomaterials 2026; 15(1) : 1-8

Progress in Biomaterials (PIBM)

https://doi.org/10.57647/pibm.2026.152605

Research Article

Sol–Gel Synthesis and Characterization of TiO_2–Doped Bioactive Glass Nanoparticles in the SiO_2–CaO–P_2O_5 System for Dental Applications

Golnaz Ghorbanipour[1], Mahboubeh A. Sharif[2,*], Masoumeh Tabatabaee[3], Mahboobeh Mahmoodi[1]

[1]*Department of Biomedical Engineering, Ya.C., Islamic Azad University, Yazd, Iran*
[2]*Department of Chemistry, Qo.C., Islamic Azad University, Qom, Iran*
[3]*Department of Chemistry, Ya.C., Islamic Azad University, Yazd, Iran*

[*]**Corresponding author:** ma.sharif@iau.ac.ir

Article History

Received:
5 January 2026

Revised:
21 February 2026

Accepted:
20 March 2026

Published in Issue:
31 March 2026

Abstract:

In this study, TiO_2–containing bioactive glass based on the SiO_2–CaO–P_2O_5 system was synthesized via the sol–gel method and heat treated at 700 °C to obtain nanoparticles. Structural, morphological, and preliminary biological evaluations were performed to investigate the effect of TiO_2 incorporation.
XRD analysis indicated a predominantly amorphous structure with broad diffraction features, consistent with nanoscale structural domains. SEM observations revealed quasi-spherical to irregular nanoparticles with particle sizes mainly below 100 nm. FTIR results confirmed the formation of a silicate-based glass network containing characteristic Si–O–Si and phosphate structural units, while spectral variations suggested successful integration of titanium species within the glass matrix. *In vitro* cytocompatibility was assessed using an MTT assay with L929 fibroblast cells. All samples exhibited high cell viability (approximately 99.5%) after 72 h of incubation, indicating the absence of detectable cytotoxic effects under the tested conditions. Overall, TiO_2 incorporation influenced the structural and morphological characteristics of the sol–gel derived bioactive glass while maintaining a predominantly amorphous structure and non-cytotoxic behavior in preliminary in vitro evaluation. Further studies are required to comprehensively assess functional performance for specific biomedical applications.

Keywords: Bioactive glass; Sol–gel method; TiO_2 incorporation; Dental applications; Cytocompatibility

Cite this article: Ghorbanipour, G., Sharif, M. A., Tabatabaee, M., Mahmoodi, M. (2026). Sol–Gel Synthesis and Characterization of TiO_2–Doped Bioactive Glass Nanoparticles in the SiO_2–CaO–P_2O_5 System for Dental Applications. *Progress in Biomaterials*, *15*(1), 1-8. https://doi.org/10.57647/pibm.2026.152605

1. Introduction

Teeth are among the most prominent components of the human body and play a significant role in social interactions by strongly influencing facial aesthetics, perceived attractiveness, and individual self-confidence. Beyond their aesthetic importance, teeth perform essential functional roles, including mastication, proper speech articulation, and maintenance of overall digestive health. Consequently, preserving dental health, structural integrity, and long-term durability has always been a fundamental objective in the field of dentistry. In recent decades, increased life expectancy and the growing expectations of patients regarding dental treatments have driven extensive efforts toward the development of materials and techniques that provide enhanced durability, adequate mechanical strength, and long-lasting aesthetic performance [1]. In this context, remarkable advances in materials science-particularly the emergence of nanotechnology-have introduced transformative opportunities in restorative and regenerative dentistry. Nanotechnology enables the design and fabrication of materials at the nanoscale, allowing the targeted enhancement of

physical, chemical, and biological properties. Nanostructured materials, owing to their high surface-to-volume ratio, increased reactivity, and improved interaction with biological tissues, have demonstrated substantial potential in improving the durability, biocompatibility, and functional performance of dental materials [2, 3]. As a result, the incorporation of nanoscale materials into dental restorations, coatings, fillers, and bioactive systems has emerged as a promising and innovative approach, leading to significant advancements in modern dentistry [4, 5, 6]. Furthermore, the complex oral environment-characterized by cyclic masticatory loads, thermal fluctuations, constant moisture, and microbial activity-necessitates the use of dental materials with high mechanical stability and chemical resistance. Therefore, dental restorative materials must not only withstand mechanical and chemical challenges but also exhibit optical properties such as color, translucency, and surface appearance that closely resemble natural tooth structure. Achieving this balance is critical for ensuring both functional longevity and patient satisfaction from an aesthetic standpoint [7]. Within this framework, biomaterials have become a central focus of contemporary dental research. Biomaterials are defined as materials capable of replacing, restoring, or enhancing the function of biological tissues while eliciting a favorable biological response and minimizing adverse tissue reactions. Recent studies have highlighted that the development of advanced dental biomaterials, particularly bioactive systems, represents a key strategy for improving the longevity and clinical performance of dental treatments. These materials can enhance restorative outcomes through the release of biologically active ions, promotion of mineral layer formation such as hydroxyapatite, and stimulation of tissue repair and regeneration processes-capabilities that are largely absent in conventional composite and ceramic materials [8, 9, 10]. Biomaterials are generally classified into three main categories: biometals, bioceramics, and biopolymers, each of which plays a distinct role in medical and dental applications based on its structural and functional characteristics. Among these groups, bioceramics have gained particular prominence in dentistry due to their excellent chemical and thermal stability, high hardness and wear resistance, favorable biocompatibility, and desirable aesthetic appearance. This category includes various bioactive ceramics such as bioactive glasses, calcium phosphate ceramics, and calcium silicates, which possess the ability to bond directly with hard tissues, facilitate bone and dental tissue regeneration, and induce favorable biological responses [5, 11, 12]. Among bioceramics, bioactive glasses represent one of the most important and extensively studied subclasses. These materials, typically based on amorphous silicate networks, exhibit a unique ability to form a direct chemical bond with hard tissues. Upon exposure to physiological or simulated body fluids, bioactive glasses undergo surface dissolution reactions that lead to the formation of a calcium-phosphate-rich layer, which subsequently crystallizes into hydroxyapatite similar to the mineral phase of bone. This mechanism underlies the bioactivity of these glasses and is responsible for their strong interfacial bonding with bone and dental tissues. Consequently, bioactive glasses have been widely employed in dental and maxillofacial applications, including bone defect repair, implant surface coatings to enhance osseointegration, dentin hypersensitivity treatment, and remineralizing dental products [13, 4]. In addition to their bioactive behavior, bioactive glasses possess osteoinductive and osteostimulatory properties, enabling them to actively promote bone formation and regeneration. The controlled release of ions such as Ca^{2+}, PO_4^{3-}, and soluble silica species ($Si(OH)_4$) not only supports hydroxyapatite formation but also activates cellular signaling pathways associated with osteogenesis. These characteristics, combined with their non-toxic, non-allergenic, and non-inflammatory nature, make bioactive glasses highly suitable candidates for clinical and biomedical applications. Recent advances in compositional design and structural engineering-such as modifying the SiO_2-CaO–Na_2O–P_2O_5 network, introducing functional dopants, and controlling amorphous or partially crystalline phases-have enabled significant improvements in mechanical properties, dissolution behavior, and biological unctionality [14, 15, 16]. In this regard, the incorporation of functional oxides such as TiO_2 has attracted considerable attention as an effective strategy to enhance the structural stability, mechanical performance, and biocompatibility of bioactive glasses. Therefore, the aim of the present study is to investigate a TiO_2-containing bioactive glass within the ternary SiO_2–CaO–P_2O_5 system and to evaluate its potential applications in dentistry. The inclusion of TiO_2 is expected to improve the durability and clinical performance of bioactive glass-based dental restorations, offering a promising pathway toward advanced biomaterials for restorative and regenerative dental applications.

2. Materials and methods

2.1 Materials

Tetraethyl orthosilicate (TEOS), calcium nitrate, triethyl phosphate (TEP), tetrabutyl orthotitanate (TBOT), and nitric acid (2 M) were used as precursor materials for the synthesis of bioactive glasses. All chemicals were of analytical grade and purchased from Merck (Germany). The tetrazolium salt (MTT) used for cytocompatibility assessment was obtained from Sigma-Aldrich (USA). All reagents were used as received without further purification. Double-distilled water was employed throughout all synthesis and solution preparation procedures.

2.2 Instruments and equipment

The structural, morphological, and biological characterizations of the synthesized bioactive glass samples were carried out using the following instruments and equipment: FT-IR analysis was performed using a Bruker Tensor 27 spectrometer (Bruker, Germany) to identify functional groups and investigate structural changes in the bioactive glass network. Phase composition and

https://doi.org/10.57647/pibm.2026.152605

structural characteristics were analyzed using an X-ray diffractometer (Bruker D8 Advance, Germany) equipped with Cu-Kα radiation (λ = 1.54 Å). The instrument was operated at an accelerating voltage of 20 kV and a current of 10 mA. The surface morphology and particle size distribution of the synthesized bioactive glass powders were examined using a scanning electron microscope (Philips XL30, Netherlands). SEM images were recorded at an accelerating voltage of 20 kV.

2.3 Synthesis of bioactive glasses by the sol–gel method

Three bioactive glass samples based on the SiO_2–CaO–P_2O_5 system (BG1, BG2, and BG3) were synthesized via the sol–gel method. The synthesis procedure was identical for all samples, with variations in precursor ratios to modify the glass composition, particularly the TiO_2 content (Table 1). Among them, the TiO_2-containing sample (BG3) was selected for detailed structural, morphological, and preliminary biological evaluations. In a typical synthesis, tetraethyl orthosilicate was hydrolyzed in 2 M nitric acid under magnetic stirring for 30 min, followed by sequential addition of calcium nitrate, triethyl phosphate, and tetrabutyl orthotitanate with continuous stirring to obtain a homogeneous sol. The sols were aged at 30 °C for 10 days, dried at 70 °C for 3 days and at 120 °C for 2 days, and finally calcined at 700 °C for 3 h to produce fine bioactive glass powders.

2.4 Preparation of simulated body fluid (SBF)

Simulated body fluid (SBF) was prepared according to the standard protocol to reproduce the ionic composition of human blood plasma. Appropriate amounts of reagent-grade inorganic salts were sequentially dissolved in double-distilled water under continuous stirring at room temperature. The pH of the solution was carefully adjusted to 7.4 at 37 °C using suitable buffering conditions. The prepared SBF was stored at 4 °C and equilibrated to 37 °C prior to use. In the present study, SBF preparation was described to indicate the physiological simulation conditions; however, no long-term immersion or quantitative mineralization analysis was performed within the scope of this work.

2.5 Structural and morphological characterization

2.5.1 Fourier transform infrared spectroscopy (FT-IR)

Fourier transform infrared (FT-IR) spectroscopy was used to identify functional groups and investigate structural changes in the synthesized bioactive glasses. For sample preparation, the bioactive glass powders were mixed with KBr at a weight ratio of 2:80 and pressed into transparent pellets. FT-IR spectra were collected in the range of 400 – 4000 cm^{-1} with appropriate resolution to detect silicate, phosphate, and Ti-related vibrational bands.

2.5.2 X-ray diffraction (XRD)

X-ray diffraction (XRD) analysis was employed to examine the phase composition and structural characteristics of the synthesized samples. Diffraction patterns were recorded over a 2θ range of 10 – 80° with a step size of 0.05°. The average crystallite size, where applicable, was estimated using the Debye–Scherrer equation to confirm nanoscale structural features.

2.5.3 Scanning electron microscopy (SEM)

Scanning electron microscopy (SEM) was used to investigate the morphology and particle size distribution of the bioactive glass powders. For SEM analysis, a small amount of powder was dispersed in ethanol using ultrasonic agitation, and a drop of the suspension was deposited onto a copper substrate and allowed to dry prior to imaging.

2.6 *In vitro* cytocompatibility assessment (MTT assay)

The cytocompatibility of the synthesized bioactive glasses was evaluated using the MTT assay as a preliminary screening of cellular response. L929 mouse fibroblast cells were seeded into 96-well plates and incubated under standard culture conditions (37 °C, 5% CO_2). After exposure to the bioactive glass samples for 72 h, MTT solution was added to each well and incubated to allow the formation of formazan crystals by metabolically active cells. The culture medium was then carefully removed, and 200 µL of dimethyl sulfoxide (DMSO) along with 25 µL of glycine–NaCl buffer was added to each well to ensure complete dissolution the formazan crystals and to stabilize the pH during absorbance measurement. The absorbance of each well was measured at 570 nm using a microplate reader. All experiments were performed in triplicate, and the results were expressed as mean values. Cell viability was calculated as a percentage relative to the negative control.

Table 1. Composition and precursor amounts of synthesized bioactive glass samples (BG1–BG3).

Sample ID	TEOS (mL)	Calcium Nitrate (g)	Triethyl Phosphate (g)	Tetrabutyl Orthotitanate (mL)	Nitric Acid (2 M) (mL)	TEOS (mL)
BG1	5.75	5.90	1.28	1.20	15	5.75
BG2	5.75	2.95	1.40	1.30	15	5.75
BG3	11.50	2.95	2.80	1.20	30	11.50

https://doi.org/10.57647/pibm.2026.152605

3. Results and discussion

3.1 Functional group analysis by FTIR

Figure 1 illustrates the FT-IR spectra of the synthesized bioactive glass samples (a) BG1, (b) BG2, and (c) BG3 recorded in the range of 400 – 4000 cm^{-1}. The spectra provide valuable information regarding the structural features and bonding configurations of the glass network as well as the effect of compositional variations among the samples. All samples exhibit a broad absorption band in the range of approximately 3200 – 3600 cm^{-1}, which is attributed to the stretching vibrations of hydroxyl (–OH) groups and adsorbed molecular water. The presence of these bands is characteristic of sol–gel derived glasses and indicates incomplete condensation of silanol groups (Si–OH) as well as moisture adsorption due to the high surface area of the powders. The bending vibration of molecular water is also observed as a weak band around 1630 – 1650 cm^{-1}. The strong absorption bands located in the region of 1000 – 1100 cm^{-1} are assigned to the asymmetric stretching vibrations of Si–O–Si bonds, confirming the formation of a silicate-based glass network. In addition, the bands observed around 800 – 820 cm^{-1} correspond to the symmetric stretching vibrations of Si–O–Si linkages, while the bands near 450 – 500 cm^{-1} are associated with bending vibrations of Si–O–Si bonds. These spectral features are typical of predominantly amorphous silicate glasses and confirm the successful formation of the glassy structure after heat treatment. The presence of phosphate groups within the glass network is evidenced by absorption bands appearing in the range of 560 – 610 cm^{-1}, attributed to the bending vibrations of P–O bonds in PO_4^{3-} units. Variations in band intensity among the samples, reflect differences in phosphate content and local structural organization within the network. Notably, BG3 exhibits subtle changes in band intensity and broadening compared to BG1 and BG2, particularly in the Si–O–Si and P–O related regions. These variations suggest structural modification of the silicate–p hosphate network upon TiO_2 incorporation. Titanium ions (Ti^{4+}) may participate in the glass network, through the formation of Ti–O–Si or Ti–O–P linkages; however, due to the overlap of Ti–O vibrational modes with silicate bands, distinct Ti-related peaks cannot be clearly resolved in the present spectra. Overall, the FT-IR results confirm the successful synthesis of predominantly amorphous bioactive glass compositions containing silicate and phosphate structural units. The observed spectral differences among BG1, BG2, and BG3 demonstrate that compositional modification, particularly TiO_2 incorporation, influences the local network structure, while maintaining the amorphous nature of the glass matrix.

3.2 Phase analysis by XRD

The X-ray diffraction (XRD) patterns of the synthesized bioactive glass samples BG1, BG2, and BG3 are presented in figure 2. All samples exhibit a broad and diffuse halo centered in the 2θ range of approximately 25 – 30°, which is a characteristic feature of amorphous silicate-based glasses. This broad diffraction feature confirms that the glass matrices of all three samples are predominantly non-crystalline after heat treatment at 700 °C. Comparison of the diffraction patterns re-

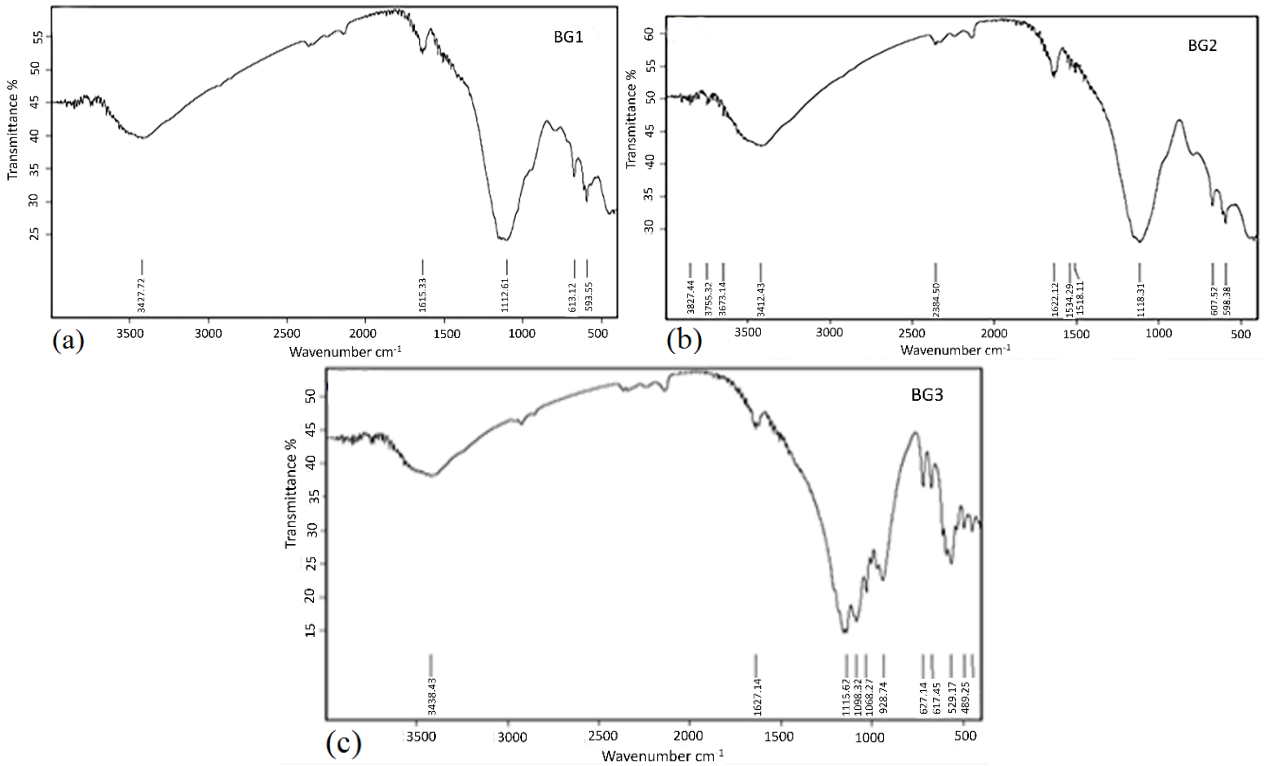

Figure 1. Illustrates the FT-IR spectra of the synthesized bioactive glass samples (a) BG1, (b) BG2, and (c) BG3.

https://doi.org/10.57647/pibm.2026.152605

veals that BG1 and BG2 display similar amorphous profiles, without sharp diffraction peaks, indicating a highly disordered glass network. In contrast, BG3 shows subtle changes in halo intensity and width, suggesting slight structural modification of the glass matrix upon TiO_2 incorporation. The absence of distinct crystalline TiO_2 peaks indicates that titanium is either present in an amorphous state or incorporated into the silicate network as a network former or intermediate oxide. Weak and broad diffraction peaks observed at approximately 38°, 48°, and 55° may correspond to limited structural ordering or partial nanocrystalline domains, as occasionally reported in sol–gel derived glass systems after thermal treatment. However, these features remain low in intensity and do not alter the predominantly amorphous character of the materials [17]. The pronounced broadening of the diffraction features suggests that any ordered domains, where present, are within the nanometer scale. The average crystallite size estimated using the Debye–Scherrer equation ($D = 0.891\lambda/\beta\cos\theta$) was approximately 60 – 100 nm, which is consistent with the nanoscale morphology observed in SEM analysis. Overall, the XRD results demonstrate that BG1, BG2, and BG3 maintain a predominantly amorphous structure following heat treatment, with only minor structural variations among compositions. TiO_2 incorporation in BG3 modifies the local structural organization while preserving the amorphous nature of the glass matrix, confirming successful compositional integration without formation of secondary crystalline TiO_2 phases.

3.3 Morphological analysis by SEM

SEM micrographs of the synthesized bioactive glass samples BG1, BG2, and BG3 are presented in figure 3. All samples exhibit nanoscale particles with predominantly quasi-spherical to irregular morphologies. Slight particle elongation and agglomeration are observed across all compositions, which is a common feature of sol–gel derived bioactive glasses and can be attributed to high surface energy and partial particle coalescence during the heat treatment process. A comparative examination of the micrographs indicates that BG1 and BG2 display relatively similar morphological characteristics, consisting of loosely agglomerated nanoparticles with irregular shapes and noticeable interparticle voids. In contrast, BG3 shows a more compact and uniform particle arrangement with slightly reduced agglomeration. This morphological variation in BG3 may be associated with TiO_2 incorporation, which can influence nucleation behavior and particle growth during sol–gel processing. Particle size analysis reveals that the nanoparticles in all samples are mainly distributed in the range of approximately 60 to 103 nm, with the majority of particles exhibiting diameters below 100 nm. BG1 and BG2 show a broader size distribution, whereas BG3 demonstrates a relatively narrower particle size range, suggesting improved control over particle growth in the presence of TiO_2. These observations are consistent with

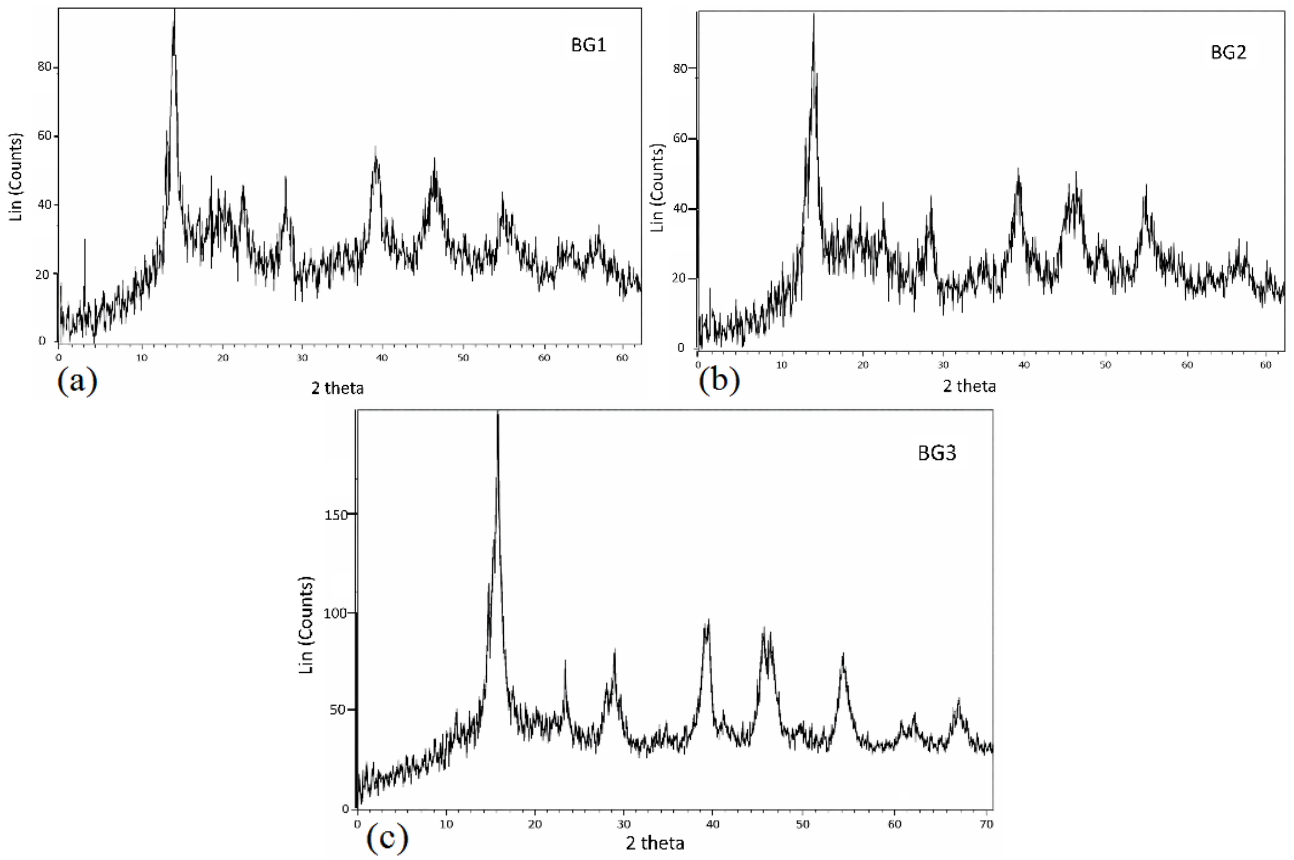

Figure 2. X-ray diffraction (XRD) pattern for bioactive glasses (a) BG1, (b) BG2, and (c) BG3 after heat treatment at 700 °C.

https://doi.org/10.57647/pibm.2026.152605

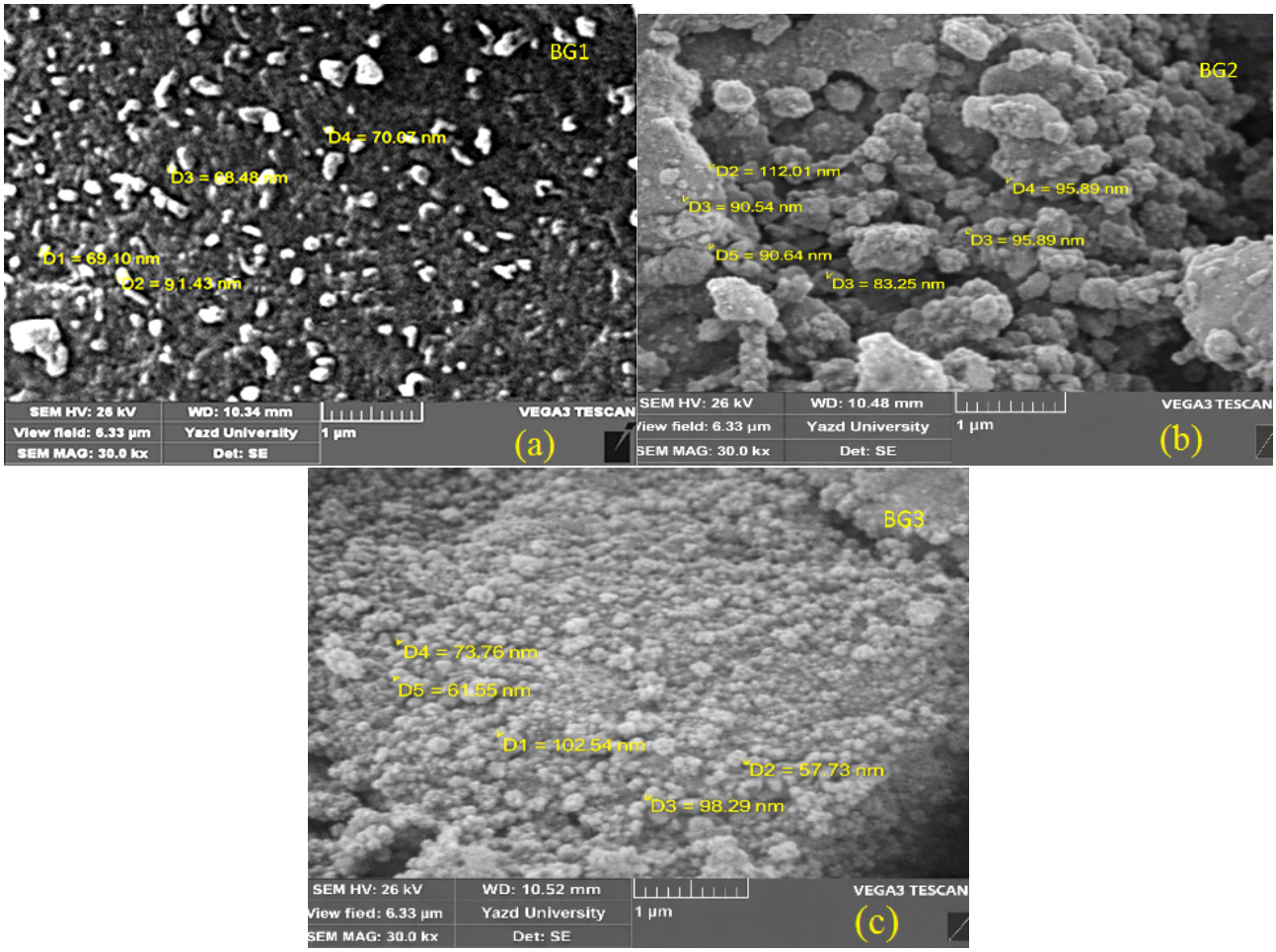

Figure 3. SEM images of bioactive glass nanoparticles (a) BG1, (b) BG2, and (c) BG3 after heat treatment at 700 °C.

the nanoscale crystallite sizes estimated from XRD analysis. Despite minor agglomeration, the nanoparticles appear reasonably well dispersed within the observed regions. Such agglomeration is typical for sol–gel derived bioactive glass nanoparticles and results from their high specific surface area. The nanoscale particle size and relatively uniform distribution observed, particularly in BG3, indicate successful synthesis of fine glass powders with controlled morphology. Overall, the SEM results confirm the formation of nanosized bioactive glass particles in all three compositions. The observed morphological differences among BG1, BG2, and BG3 demonstrate that compositional modification, especially TiO_2 incorporation, influences particle morphology and size.

3.4 *In vitro* cytocompatibility assessment (MTT assay)

The *in vitro* cytocompatibility of the synthesized bioactive glass nanoparticles BG1, BG2, and BG3 was evaluated using L929 fibroblast cells by means of the MTT assay as a preliminary assessment of cellular response. Cells were incubated with the bioactive glass samples for 72 h, and cell viability was quantified relative to the untreated control group. The percentage of viable cells following exposure to each sample is presented in figure 4. The results indicate that all three samples exhibited high cell viability, with no statistically significant difference compared to the control group. Cell viability values for BG1, BG2, and BG3 remained above 95%, demonstrating that none of the synthesized bioactive glass compositions induced detectable cytotoxic effects under the experimental conditions. Comparative analysis among the samples shows that BG3, which contains TiO_2, exhibited cell viability comparable to that of BG1 and BG2. This observation suggests that the TiO_2 incorporation does not negatively influence short-term cellular metabolic activity in L929 fibroblasts. It should be noted that the MTT assay evaluates mitochondrial metabolic activity as an indicator of cell viability and does not provide comprehensive information regarding long-term cellular behavior, proliferation, or differentiation. Within the limitations of this assay, the results demonstrate that the synthesized sol–gel derived bioactive glass nanoparticles are non-cytotoxic under the tested in vitro conditions. Overall, the MTT findings support the preliminary cytocompatibility of the investigated compositions and indicate that TiO_2 incorporation does not adversely affect short-term cellular response.

https://doi.org/10.57647/pibm.2026.152605

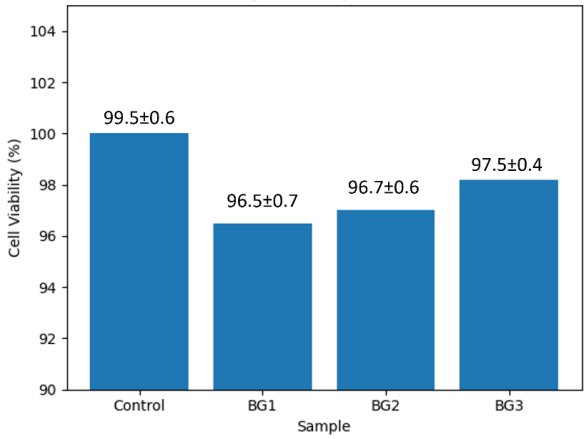

Figure 4. Cell viability of L929 fibroblast cells after 72 h incubation with bioactive glass nanoparticles (MTT assay).

4. Conclusions

The *in vitro* cytocompatibility of the synthesized bioactive glass nanoparticles BG1, BG2, and BG3 was evaluated using L929 fibroblast cells by means of the MTT assay as a preliminary assessment of cellular response. Cells were incubated with the bioactive glass samples for 72 h, and cell viability was quantified relative to the untreated control group. The percentage of viable cells following exposure to each sample is presented in figure 4. The results indicate that all three samples exhibited high cell viability, with no statistically significant difference compared to the control group. Cell viability values for BG1, BG2, and BG3 remained above 95%, demonstrating that none of the synthesized bioactive glass compositions induced detectable cytotoxic effects under the experimental conditions. Comparative analysis among the samples shows that BG3, which contains TiO_2, exhibited cell viability comparable to that of BG1 and BG2. This observation suggests that the TiO_2 incorporation does not negatively influence short-term cellular metabolic activity in L929 fibroblasts.

It should be noted that the MTT assay evaluates mitochondrial metabolic activity as an indicator of cell viability and does not provide comprehensive information regarding long-term cellular behavior, proliferation, or differentiation. Within the limitations of this assay, the results demonstrate that the synthesized sol–gel derived bioactive glass nanoparticles are non-cytotoxic under the tested *in vitro* conditions. Overall, the MTT findings support the preliminary cytocompatibility of the investigated compositions and indicate that TiO_2 incorporation does not adversely affect short-term cellular response.

Acknowledgements
The authors would like to thank Islamic Azad University, Yazd Branch, for their financial support throughout this research.

Authors contributions
All authors contributed equally to the conception, design, execution, and writing of this work. All authors read and approved the final manuscript.

Availability of data and materials
The datasets generated during and/or analyzed during the current study are available from the corresponding author on reasonable request.

Conflict of interests
The authors declare that they have no known competing financial interests or personal relationships that could have appeared to influence the work reported in this paper.

References

1. Dipalma G, Inchingolo AD, Guglielmo M, Morolla R, Palumbo I, Riccaldo L, Mancini A, Palermo A, Malcangi G, Inchigolo AM, and Inchingolo F. Nanotechnology and its application in dentistry: A systematic review of recent advances and innovations. Journal of Clinical Medicine 2024; 13:5268. DOI: 10.3390/jcm13175268
2. Chaudhary N, Chaudhary V, Bansal M, Karol M, Singh G, Kumawat S, Sharma S, and Jain H. Nanotechnology in restorative dentistry: A review. International Journal of Applied Dental Sciences 2024; 10:192–195
3. Aktas OC, Puchert K, Vurucu EE, Ersöz B, Veziroglu S, and Sen S. A review on nanocomposite coatings in dentistry. Journal of Materials Science 2024; 59:17991–18008
4. Skallevold HE, Rokaya D, Khurshid Z, and Zafar MS. Bioactive glass applications in dentistry. International Journal of Molecular Sciences 2019; 20:5960. DOI: 10.3390/ijms20235960
5. Jafari N, Seyed Habashi M, Hashemi A, Shirazi R, Tanideh N, and Tamadon A. Application of bioactive glasses in various dental fields. Biomaterials Research 2022; 26:31. DOI: 10.1186/s40824-022-00274-6
6. Gao Y, Seles MA, and Rajan M. Role of bioglass derivatives in tissue regeneration and repair: A review. Reviews on Advanced Materials Science 2023; 62:20220318
7. Woźniak-Budych MJ, Staszak M, and Staszak K. A critical review of dental biomaterials with an emphasis on biocompatibility. Biomaterials for Dental Applications 2023; 60:709–39. DOI: 10.17219/dmp/172732
8. Gil-Marques B, Pallarés-Sabater A, Brizuela-Velasco A, Sánchez Lasheras F, Lázaro-Calvo P, Gómez-Adrián MD, and Larrazábal-Morón C. A biomechanical analysis of the influence of the morphology of bone block grafts on load transfer using finite element methods. Materials 2022; 15:9039. DOI: 10.3390/ma15249039

9. Vaiani L, Boccaccio A, Uva AE, Palumbo G, Piccininni A, Guglielmi P, Cantore S, Santacroce L, Charitos IA, and Ballini A. Ceramic materials for biomedical applications: An overview on properties and fabrication processes. Journal of Functional Biomaterials 2023; 14:146. DOI: 10.3390/jfb14030146
10. Yu H, Yao J, Du Z, Guo J, and Lei W. Comparative evaluation of mechanical properties and color stability of dental resin composites for chairside provisional restorations. Polymers 2024; 16:2089. DOI: 10.3390/polym16142089
11. Wang J, Zhang L, and Wang K. Bioactive ceramic-based materials: Beneficial properties and potential applications in dental repair and regeneration. Regenerative Medicine 2024; 19:257–278. DOI: 10.1080/17460751.2024.2343555
12. Surana P, Dhull KS, Arya A, Samreen S, Rajan M, and Parihar AS. Bio-ceramics application in dentistry. Bioinformation 2024; 20:136–139
13. Välimäki VV and Aro HT. Molecular basis for action of bioactive glasses as bone graft substitutes. Scandinavian Journal of Surgery 2006; 95:95–102
14. Hoppe A and Boccaccini AR. Biological impact of bioactive glasses and their dissolution products. Frontiers in Oral Biology 2015; 17:22–32. DOI: 10.1159/000381690
15. Bargavi P, Chitra S, Durgalakshmi D, Rajashree P, and Balakumar S. Effect of titania concentration in bioglass/TiO_2 nanostructures and in vitro biological assessment. Journal of Nanoscience and Nanotechnology 2018; 18:4746–4754. DOI: 10.1166/jnn.2018.15340
16. Deshmukh K, Kovařík T, Krenek T, Docheva D, Stich T, and Pola J. Recent advances and future perspectives of sol–gel derived porous bioactive glasses: A review. RSC Advances 2020; 10:33782. DOI: 10.1039/D0RA04287K
17. Catauro M, Bollino F, Renella RA, and Papale F. Sol–gel synthesis of SiO_2–CaO–P_2O_5 glasses: Influence of the heat treatment on their bioactivity and biocompatibility. Ceramics International 2015; 41:12578–12588